Original Article

Renal Fibrosis and Glomerulosclerosis in a New Mouse Model of Diabetic Nephropathy and Its Regression by Bone Morphogenic Protein-7 and Advanced Glycation End Product Inhibitors

Hikaru Sugimoto,[1] Gordan Grahovac,[1] Michael Zeisberg,[1] and Raghu Kalluri[1,2,3]

Diabetic nephropathy is currently the most common cause of end-stage renal disease (ESRD) in the western world. A mouse model for diabetic nephropathy that encompasses the salient features of this disease in the kidney is not available. Here, we report that CD1 mice, in contrast to inbred C57BL/6 and 129Sv strains, develop ESRD associated with prominent tubulointerstitial nephritis and fibrosis within 3 months and die because of diabetic complications by 6–7 months after a single injection of streptozotocin. Histopathologic lesions observed in these mice mimic human diabetic nephropathy, including glomerular hypertrophy, diffuse glomerulosclerosis, tubular atrophy, interstitial fibrosis, and decreased renal excretory function. Next, we tested the therapeutic efficacy of bone morphogenic protein-7 (BMP-7) and inhibitors of advanced glycation end products (AGEs), aminoguanidine and pyridoxamine, to inhibit and regress the progression of renal disease in diabetic CD1 mice. We demonstrate that although aminoguanidine, pyridoxamine, and BMP-7 significantly inhibit glomerular lesions, BMP-7 is most effective in the inhibition of tubular inflammation and tubulointerstitial fibrosis in these mice. Collectively, our results report a new mouse model for diabetic nephropathy with prominent interstitial inflammation and fibrosis and the selective inhibition of diabetic kidney disease by AGE inhibitors and BMP-7.
***Diabetes* 56:1825–1833, 2007**

Diabetic nephropathy is the single most common cause of end-stage renal disease (ESRD) in the U.S., Europe, and Japan. It is responsible for about one-third of patients with ESRD, with the cost of health care for these patients being projected at $12 billion per year in the U.S. by 2010 (1). Specific therapies to inhibit or reverse progression of advanced stages of diabetic nephropathy associated with interstitial fibrosis are not available, and effective management of blood glucose levels and/or hypertension yet remain the only therapeutic options (2,3).

A major difficulty in the study of diabetic nephropathy has been the lack of a representative mouse model that develops ESRD associated with tubulointerstitial fibrosis (4). Various inbred mouse strains develop glomerular lesions (representative of early stages of human diabetic nephropathy), but none of them develops prominent ESRD mimicking advanced stages of human diabetic nephropathy (4).

In humans, diabetic nephropathy manifests as a clinical syndrome consisting of albuminuria, progressive decline in excretory renal function, and an increased risk for cardiovascular disease (5). Diabetic albuminuria in humans is associated with the development of characteristic histopathologic features, including glomerular hypertrophy, thickening of the glomerular basement membrane, and mesangial matrix expansion (6). Decline of excretory renal function is associated with glomerulosclerosis and tubulointerstitial fibrosis (6). A mouse model that develops all of these features is not currently available (4).

Here we demonstrate that CD1 mice recapitulate several features of human diabetic nephropathy in 6 months after a single injection of streptozotocin (STZ). These mice exhibit tubulointerstitial fibrosis and decreased excretory renal function, in contrast to C57BL/6 and 129Sv mice injected with STZ, which exhibit a milder disease form. We further demonstrate that administration of aminoguanidine and pyridoxamine, two inhibitors of advanced glycation end product (AGE) accumulation, as well as administration of recombinant human bone morphogenic protein-7 (rhBMP-7), regress progression of diabetic nephropathy in diabetic CD1 mice.

RESEARCH DESIGN AND METHODS

We purchased 7-week-old C57BL/6, 129Sv, and CD1 mice from Charles River (Wilmington, MA). These mice received standard chow and water. Blood

From the [1]Division of Matrix Biology, Department of Medicine, Beth Israel Deaconess Medical Center and Harvard Medical School, Boston, Massachusetts; the [2]Department of Biological Chemistry and Molecular Pharmacology, Harvard Medical School, Boston, Massachusetts; and the [3]Harvard–Massachusetts Institute of Technology Division of Health Sciences and Technology, Boston, Massachusetts.

Address correspondence and reprint requests to Raghu Kalluri, Associate Professor of Medicine, Harvard Medical School, Chief, Division of Matrix Biology, Department of Medicine, RW 514, Beth Israel Deaconess Medical Center, 330 Brookline Ave., Boston, MA 02215. E-mail: rkalluri@bidmc.harvard.edu.

Received for publication 1 September 2006 and accepted in revised form 16 April 2007.

Published ahead of print at http://diabetes.diabetesjournals.org on 24 April 2007. DOI: 10.2337/db06-1226.

AGE, advanced glycation end product; BMP, bone morphogenic protein; CML, carboxymethyllysine; ESRD, end-stage renal disease; FSP1, fibroblast-specific protein 1; PAS, periodic acid Schiff; rhBMP, recombinant human BMP; STZ, streptozotocin; TGF, transforming growth factor.

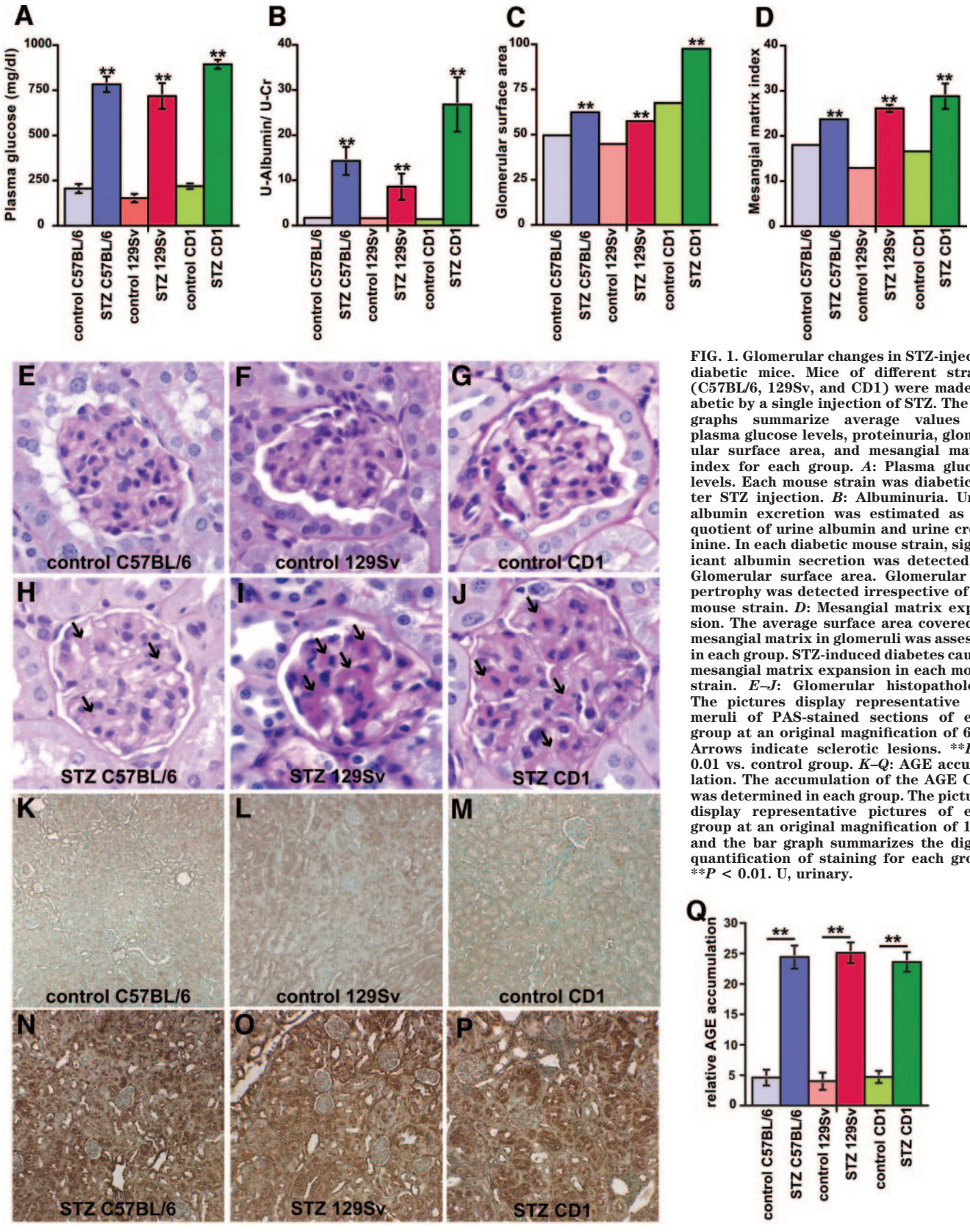

FIG. 1. Glomerular changes in STZ-injected diabetic mice. Mice of different strains (C57BL/6, 129Sv, and CD1) were made diabetic by a single injection of STZ. The bar graphs summarize average values for plasma glucose levels, proteinuria, glomerular surface area, and mesangial matrix index for each group. *A*: Plasma glucose levels. Each mouse strain was diabetic after STZ injection. *B*: Albuminuria. Urine albumin excretion was estimated as the quotient of urine albumin and urine creatinine. In each diabetic mouse strain, significant albumin secretion was detected. *C*: Glomerular surface area. Glomerular hypertrophy was detected irrespective of the mouse strain. *D*: Mesangial matrix expansion. The average surface area covered by mesangial matrix in glomeruli was assessed in each group. STZ-induced diabetes caused mesangial matrix expansion in each mouse strain. *E–J*: Glomerular histopathology. The pictures display representative glomeruli of PAS-stained sections of each group at an original magnification of 63×. Arrows indicate sclerotic lesions. **P < 0.01 vs. control group. *K–Q*: AGE accumulation. The accumulation of the AGE CML was determined in each group. The pictures display representative pictures of each group at an original magnification of 10×, and the bar graph summarizes the digital quantification of staining for each group. **P < 0.01. U, urinary.

samples were collected between 12 and 1 P.M., and plasma glucose was measured by the glucose oxidase method.

STZ administration into different strains of mice and therapy of diabetic CD1 mice. Diabetes was induced in 8-week-old C57BL/6, 129Sv, and CD1 mice by an injection of STZ. CD1 and C57BL/6 mice were made diabetic by single intraperitoneal injection of STZ at 200 mg/kg in 10 mmol/l citrate buffer (pH 4.5). For 129Sv mice, 50 mg/kg of STZ was injected intraperitoneally for 5 consecutive days. Citrate buffer was injected as a control arm of the experiments. At 3 days after the STZ injection, diabetes was confirmed by a urine dipstick method, and mice were divided into experimental study groups. In each of the mouse strains, mortality was ~30% with a peak at 3.5 months. Diabetic and nondiabetic CD1 mice were killed at 3.5 and 6 months after the

injection of STZ. Diabetic and nondiabetic C57BL/6 and 129Sv mice were killed at 6 months after the STZ injection. Diabetic CD1 mice were randomly divided into four groups and treated with the following three compounds, starting 1 month after STZ injection for 5 months thereafter. Aminoguanidine ($n = 8$; Sigma, St. Louis, MO) and pyridoxamine dihydrochloride ($n = 6$; Sigma) were dissolved in drinking water at a concentration of 1 and 2g/l, respectively (7,8). rhBMP-7 was injected into four diabetic mice at a dose of 300 μg/kg every other day (9). Seven diabetic mice injected with vehicle buffer every other day served as a control. On death at 6 months, renal tissues were evaluated by morphometric analysis for mesangial expansion, interstitial fibrosis, tubular atrophy, and interstitial fibroblast accumulation. In all groups (treated and untreated), the mortality was ~30% between 2 and 4 months after the single STZ injection. Deaths before 2 months were not noted in any groups. All mouse studies were reviewed and approved by the institutional animal care and use committee.

Renal functional analysis. Spot urine samples were collected and urinary albumin and creatinine concentration estimated using a bromocresol green–based colorimetric assay according to the manufacturer's recommendation (Sigma). Urine albumin excretion was estimated as the quotient of urine albumin and urine creatinine as described in our previous publications (10,11). Clinical chemistry analysis of plasma was performed by Antech Diagnostics (Boston, MA).

Histological assessment of renal injury. Renal cross sections were fixed in 4% paraformaldehyde, embedded in paraffin, and deparaffinized in xylene, and then 4-μm sections were stained with hematoxylin-eosin, periodic acid Schiff (PAS), and Masson trichrome. The extent of renal injury was assessed by morphometric analysis of the glomerular disease, tubular damage, and interstitial fibrosis as previously described (12). For glomerular damage, we evaluated mesangial expansion and enlargement of the glomeruli. A point-counting method was used to quantify mesangial matrix deposition according to a previous method with some modifications (13). We analyzed 20 PAS-stained glomeruli from each mouse on a digital microscope screen grid containing 667 (29×23) points. The number of grid points that hit pink or red mesangial matrix deposition were divided by the total number of points in the glomerulus to obtain the percentage of mesangial matrix deposition (mesangial matrix index) in a given glomerulus. The relative interstitial volume was evaluated by morphometric analysis using a 10-μm graticule fitted into the eyepiece of the microscope. We evaluated 10 randomly selected cortical areas under 200× magnification for each mouse. Tubules were evaluated for their widened lumen, atrophy, or thickened basement membranes to estimate the percentage of damaged tubules (% tubular damage) (9).

Immunostaining. Indirect immunofluorescence studies were performed as described previously (14). Briefly, 4-μm cryosections were fixed in acetone for 5 min at 4°C. To block the nonspecific antibody bindings, 1% BSA in 10 mmol/l PBS were applied for 20 min at room temperature. As primary antibodies, we used a rabbit antibody to S100-A4 as a fibroblast marker (Dako, Carpinteria, CA), goat anti–collagen III antibody (Southern Biotechnology Associates, Birmingham, AL), and goat anti–transforming growth factor (TGF)-β1 antibody (Santa Cruz Biotechnology, Santa Cruz, CA). As secondary antibodies, fluorescein isothiocyanate–conjugated anti-goat IgG and anti-rabbit IgG were obtained from Jackson ImmunoResearch (West Grove, PA). The primary antibodies were applied for 1 h at room temperature followed by incubation with secondary antibodies. For AGE staining, 4% paraformaldehyde–fixed paraffin-embedded sections were stained with a CSAII biotin–free tyramide signal amplification system according to the manufacturer's recommendations (Dako). Primary antibodies against carboxymethyllysine (CML; Wako Chemical, Richmond, CA) were used.

Digital quantification. After frozen renal sections were labeled using antibodies specific to TGF-β1, collagen III, or CML, photomicrographs from a mouse kidney cortex were taken using 100× magnification under an Axioscope 2 Plus fluorescence microscope (Carl Zeiss Micro Imaging, Thornwood, NY). The cortical TGF-β1–positive tubular areas were measured by Carl Zeiss Axiovision digital imaging software. The TGF-β1–positive area was divided by the total cortical area to obtain the percentage of TGF-β1–positive area. We evaluated ~300–600 tubules in the cortex for each mouse kidney. For quantification of collagen III and CML, five 100× magnification pictures from each mouse were assessed with National Institutes of Health Image J software.

Statistical analysis. Values are the means ± SE. The significance of the differences between the two groups was analyzed by Student's t test. Comparisons among three groups were performed by two-way ANOVA followed by Sheffe's test to evaluate the significance of the differences between any two groups. A level of $P < 0.05$ was defined as statistically significant.

RESULTS

Renal histopathology in diabetic C57BL/6, 129Sv, and CD1 mice. To establish a model of STZ-induced type 1 diabetes, a single injection of STZ is used to elicit diabetes secondary to its toxicity to the pancreatic β-cells (4,15). Eight-week-old C57BL/6, 129Sv, and CD1 mice were made diabetic by intraperitoneal injection of STZ. All diabetic mice were severely hyperglycemic at the time of death, and plasma glucose levels were elevated in all mouse strains (Fig. 1*A*). Urine protein excretion (estimated as the urine albumin–to–urine creatinine ratio) was evaluated at the time of death, and all three strains of mice had significant proteinuria (Fig. 1*B*), similar to humans with diabetic nephropathy.

In human diabetic nephropathy, renal histopathologic findings include diffuse thickening of the glomerular basement membrane, prominent mesangial expansion, nodular lesions in the periphery of glomerular tufts, and tubulointerstitial fibrosis (16–18). Glomerular morphometric analysis demonstrates that diabetic C57BL/6, 129Sv, and CD1 mice develop glomerular hypertrophy, confirming previous studies (19,20) (Fig. 1*C*). CD1 mice exhibited the most prominent glomerular lesions and mesangial matrix deposition compared with C57BL/6 and 129Sv mice with diabetes. Control experiments in which kidney sections were labeled with antibodies specific to CML revealed that in each mouse strain AGE deposition was significantly increased in the STZ-injected diabetic mice. AGE levels did not differ significantly between the diabetic mouse strains (Fig. 1*K*–*Q*).

Tubular injury associated with diabetic nephropathy in humans is characterized by widened lumina, flattened tubular cells, and thickened tubular basement membranes. Tubular injury was present in all diabetic mouse strains (Fig. 2*A*–*G*). C57BL/6 mice and 129Sv mice did not develop interstitial fibrosis, again confirming previous studies (4). Diabetic CD1 mice, however, exhibited significant interstitial fibrosis at 6 months of diabetes (Figs. 2*H* and *N*). Analysis of kidneys from diabetic CD1 mice collected at earlier time points (3.5 months) revealed mild tubulointerstitial fibrosis (data not shown) (21).

Tubulointerstitial fibrosis in diabetic CD1 mice. After 6 months of diabetes caused by STZ injection, significant widening of the interstitial space associated with collagen accumulation was observed (Fig. 3*A*). Tubular damage included a loss of eosinophilic pink staining in the tubular cytoplasm (reminiscent of the Armanni-Ebstein anomaly observed in human diabetic nephropathy patients) (Fig. 3*B*) and atrophy of renal tubules, preferentially restricted to the cortical regions (Fig. 3*C*). The most frequently seen tubular damage was cyst-like enlargement of tubular lumen (Fig. 3*C*). Diabetic CD1 mice presented with a diffuse glomerulosclerosis with minimal focal glomerulosclerosis (Fig. 3*D*). Increased interstitial volume in diabetic CD1 mice was associated with increased accumulation of fibroblasts, as evaluated by labeling with antibodies to fibroblast-specific protein 1 (FSP1) (Fig. 3*E* and *F*). TGF-β1 is a mediator of progressive renal disease in experimental diabetic mice (22,23). Immunolabeling using specific antibodies to TGF-β1 revealed a significant increase of TGF-β1 in the tubulointerstitium of diabetic CD1 mice compared with nondiabetic control mice (Fig. 3*H* and *I*). Tubulointerstitial fibrosis in CD1 mice correlated with decreased renal excretory function in diabetic CD1 mice (Table 1). Plasma creatinine levels increased from 0.58 mg/dl (in

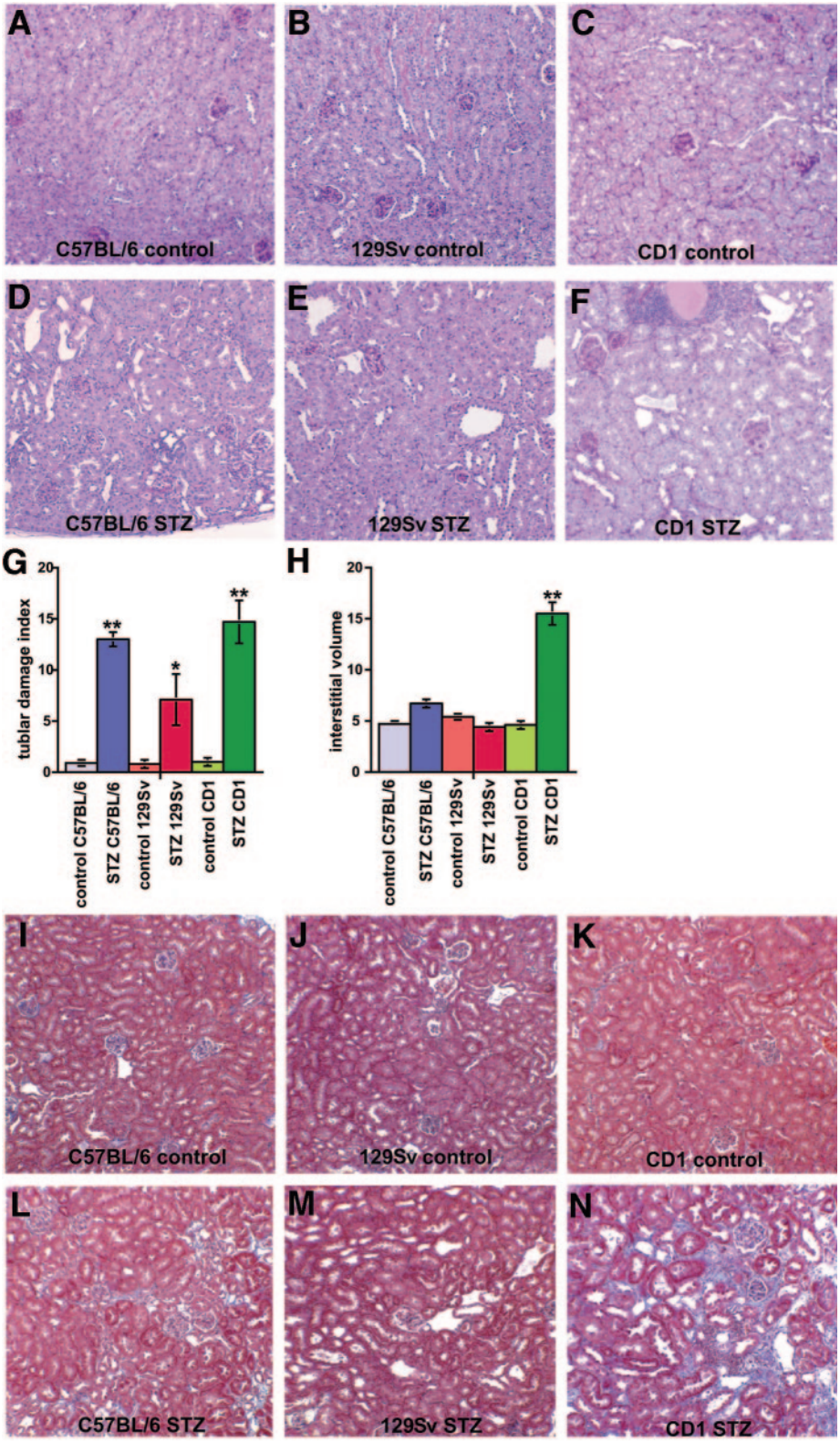

FIG. 2. STZ-induced diabetes causes tubulointerstitial fibrosis in CD1 mice. *A–G*: Tubular atrophy. Tubules in PAS-stained sections were evaluated for their widened lumen, atrophy, or thickened basement membranes. The bar graph summarizes the percentage of damaged tubules in each group, and the pictures display representative kidney sections of each group at an original magnification of 10×. *H–N*: Interstitial fibrosis. The relative interstitial volume was quantified by morphometric analysis in Masson trichrome–stained kidney sections in each group. The bar graph summarizes average values for each group, and the pictures display representative areas of Masson trichrome–stained kidneys at a magnification of 10×. Significant interstitial fibrosis was exclusively present in diabetic CD1 mice. *$P < 0.05$, **$P < 0.01$ vs. control group.

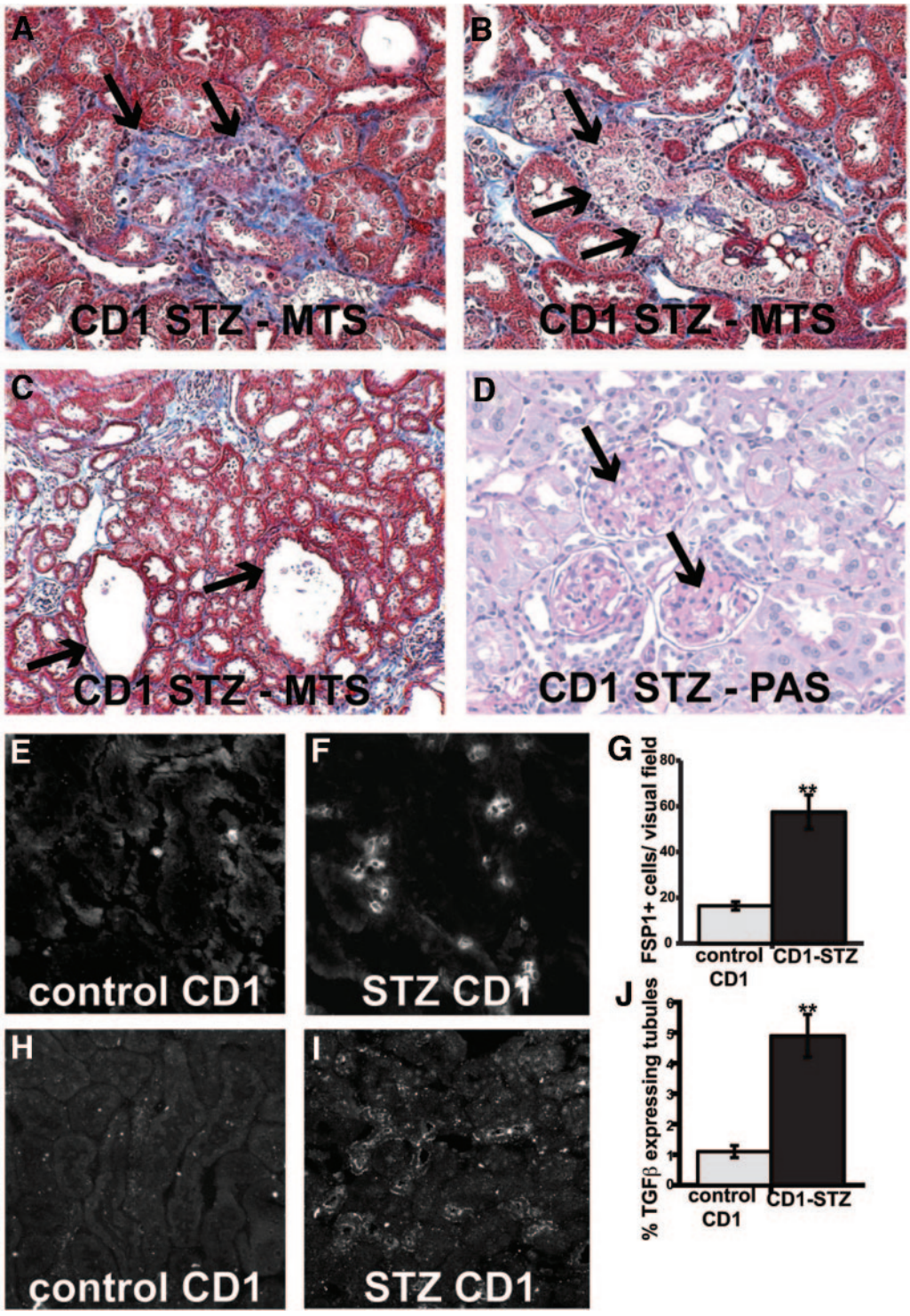

FIG. 3. Renal histopathology of STZ-injected diabetic CD1 mice. *A*: Interstitial fibrosis. Masson trichrome staining reveals collagen deposition (blue color, arrows) in the widened interstitium of STZ-injected diabetic mice. *B*: Tubular glycogen deposition. In kidneys from STZ-injected mice, tubules mimicking the Armanni-Ebstein anomaly (arrows), which is commonly observed in patients with diabetic nephropathy, are present. *C*: Tubular cysts. STZ-induced diabetic nephropathy is associated with tubular cysts (arrows). *D*: Glomerulosclerosis. Diffuse glomerulosclerosis (arrows) is the predominant glomerular pathology in STZ-injected CD1 mice. We did not observe focal glomerulosclerotic lesions. *E–G*: FSP1-positive fibroblasts. We stained kidney sections from control and diabetic CD1 mice with antibodies specific for the fibroblast marker FSP1. The pictures display representative photomicrographs of FSP1-stained kidneys, and the bar graph displays average numbers of FSP1-positive fibroblasts. There is a significant accumulation of FSP1-positive fibroblasts in diabetic CD1 mice. *H–J*: Tubular TGF-β1 expression. Kidney sections from control and diabetic CD1 mice were stained with TGF-β1 antibodies. Tubular TGF-β1 expression is significantly increased in diabetic CD1 mice. The pictures display representative stainings, and the bar graph summarizes the quantitative analysis. **$P < 0.01$ vs. control group.

TABLE 1
Clinical chemistry analysis of plasma from control and diabetic CD1 mice

	Nondiabetic	Diabetic
Plasma creatinine (mg/dl)	0.58 ± 0.18	1.6 ± 0.17*
Total protein (g/dl)	5.25 ± 0.29	5.08 ± 0.29
Albumin (g/dl)	2.65 ± 0.17	2.48 ± 0.04
ALP (U/l)	33 ± 3	137 ± 26*
Na (mEq/l)	143 ± 5	138 ± 3
K (mEq/l)	7.9 ± 0.3	9.9 ± 0.3*
P (mg/dl)	8.6 ± 0.3	9.4 ± 0.7
Total cholesterol (mg/dl)	138 ± 19	202 ± 25
Triglyceride(mg/dl)	137 ± 19	863 ± 177*
Plasma osmolarity (mOsm/l)	304 ± 106	334 ± 6*

Data are means ± SE. *$P < 0.05$. ALP, alkaline phosphate.

nondiabetic control mice) to 1.6 ± 0.17 mg/dl (in diabetic CD1 mice) after 6 months of STZ-induced diabetes (Table 1). Increased plasma creatinine levels were associated with increased potassium and phosphate levels (Table 1).

Aminoguanidine, pyridoxamine, and rhBMP-7 ameliorate progression of interstitial fibrosis in diabetic CD1 mice. Diabetic CD1 mice develop chronic renal disease associated with tubulointerstitial fibrosis associated with decreased excretory renal function. Therefore, we next tested the efficacy of three different experimental therapeutics to inhibit the progression of renal disease in these mice. AGEs (products of the nonenzymatic reaction of amino groups in proteins and lipids with reducing sugars such as glucose) are considered to be important for the progression of diabetic nephropathy. Here, we used two different inhibitors of AGE accumulation, aminoguanidine and pyridoxamine, to address their therapeutic benefit. Pyridoxamine is shown to inhibit the accumulation of AGE by inhibiting conversion of Amadori intermediate to AGEs through binding of redox metal ions (24,25). Aminoguanidine has been suggested to facilitate cross-link cleavage of AGEs, leaving uncomplexed AGE, and facilitating excretion by the kidney (22).

BMP-7 (rhBMP-7) is a growth factor of the TGF-β superfamily, and several independent studies demonstrate that administration of rhBMP-7 inhibits progression of renal fibrosis in animal models for chronic renal disease (9,12,26,27). Antifibrotic action of BMP-7 is mediated via direct antagonism of TGF-β1 signaling (12,28,29). Previous studies suggest a therapeutic benefit for rhBMP-7 in a rat model of STZ-induced diabetic glomerulosclerosis (which do not develop interstitial fibrosis) (30).

In our study, aminoguanidine and pyridoxamine inhibited glomerular hypertrophy and mesangial matrix expansion (Fig. 4), confirming that AGEs are involved in the progression of glomerular lesions associated with diabetic nephropathy. Efficacy of aminoguanidine and pyridoxamine in these studies further confirms that renal fibrosis observed in diabetic CD1 mice is not caused by nonspecific toxicity of STZ (4). Administration of rhBMP-7 significantly inhibited glomerular hypertrophy but had an insignificant effect on mesangial matrix expansion and proteinuria (Fig. 4). However, administration of rhBMP-7 was most effective in inhibiting tubulointerstitial fibrosis (Figs. 5 and 6). Mechanisms of action for AGE inhibitors and rhBMP-7 were confirmed by immunolabeling using antibodies specific for the AGE CML. Although both pyridoxamine and aminoguanidine significantly decreased CML accumulation, administration of rhBMP-7 had no

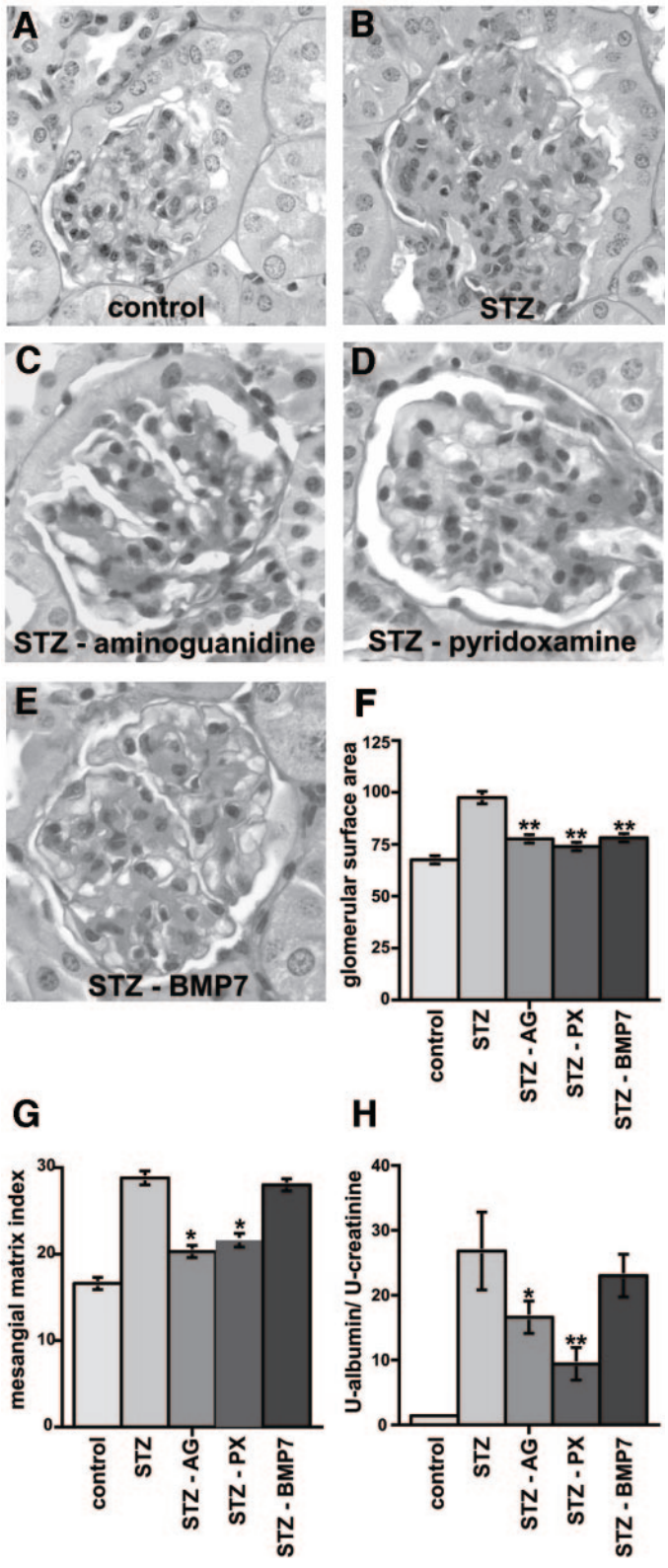

FIG. 4. Inhibition of glomerulosclerosis in STZ-injected CD1 mice. We compared glomerular pathologies between nondiabetic CD1 mice (control), STZ-injected diabetic CD1 mice, and STZ-injected diabetic CD1 mice that received either aminoguanidine, pyridoxamine, or rhBMP-7. *A–E*: The pictures display representative glomeruli of PAS-stained kidney sections of each group at a magnification of 63×. *F–H*: The bar graphs display average values for glomerular surface area, mesangial matrix expansion, and albuminuria of each group. *$P < 0.05$, **$P < 0.01$ vs. STZ group. AG, aminoguanidine; PX, pyridoxamine; U, urinary.

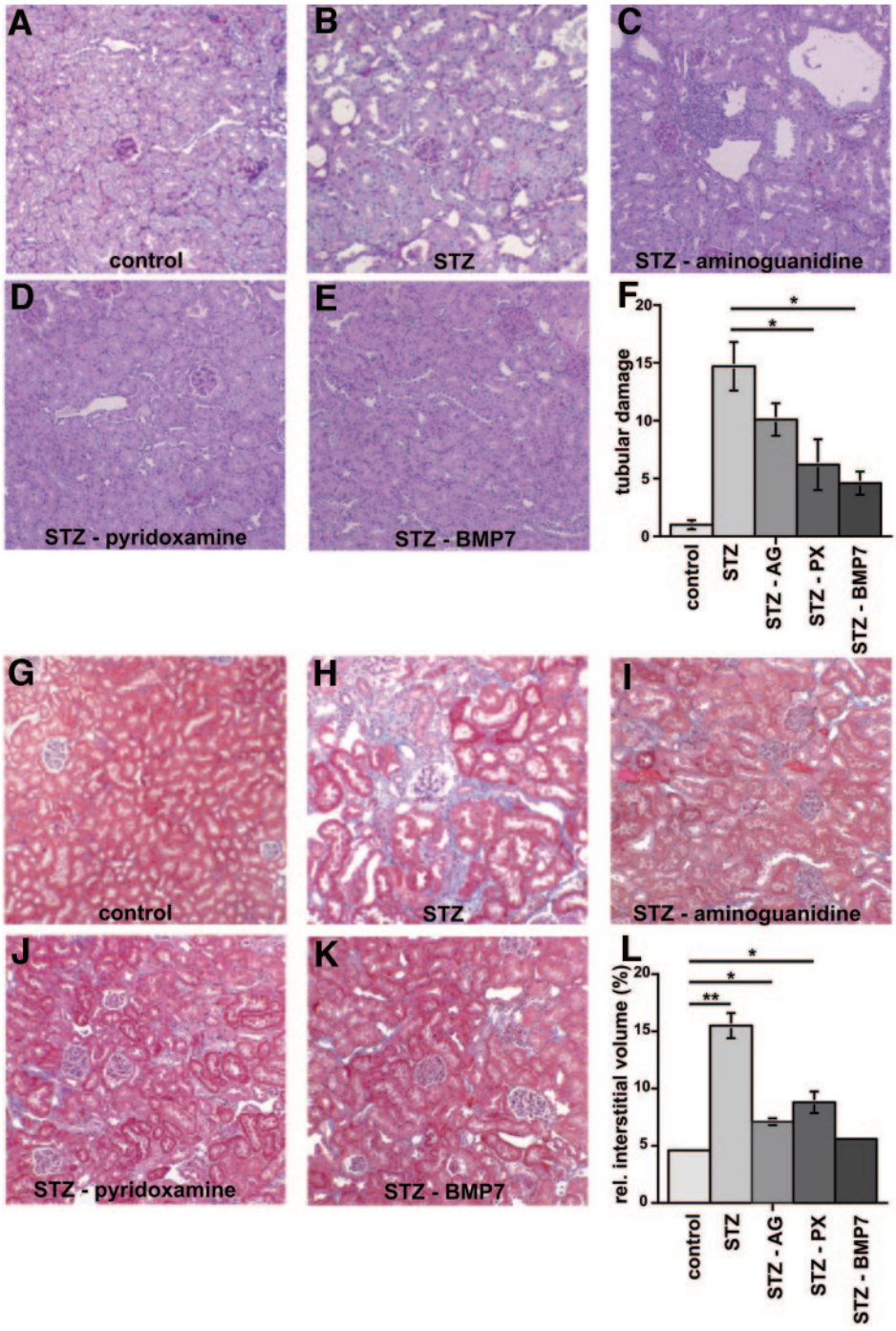

FIG. 5. Inhibition of tubulointerstitial fibrosis in STZ-injected diabetic CD1 mice. We compared tubulointerstitial fibrosis between nondiabetic CD1 mice (control), STZ-injected diabetic CD1 mice, and STZ-injected diabetic CD1 mice that received either aminoguanidine, pyridoxamine, or rhBMP-7. *A–F*: Tubular damage. Tubules in PAS-stained sections were evaluated for their widened lumen, atrophy, or thickened basement membranes. The bar graph summarizes the percentage of damaged tubules in each group, and the pictures display representative kidney sections of each group at an original magnification of 10×. *$P < 0.05$, **$P < 0.01$ vs. STZ group. *G–L*: Interstitial fibrosis. The relative interstitial volume was quantified by morphometric analysis in Masson trichrome–stained kidney sections in each group. The bar graph summarizes average values for each group, and the pictures display representative areas of Masson trichrome–stained kidneys at a magnification of 10×. *$P < 0.05$, **$P < 0.01$ vs. normoglycemic control group. *M*: Serum creatinine. Inhibition of tubulointerstitial fibrosis in diabetic CD1 mice correlated with decreased serum creatinine levels compared with untreated control diabetic CD1 mice. AG, aminoguanidine; PX, pyridoxamine.

significant impact (Fig. 7). Body weight at the conclusion of the studies (STZ 30.0 ± 0.9 g, STZ-aminoguanidine 28.9 ± 0.7 g, STZ-pyridoxamine 28.4 ± 1.0 g, and STZ–rhBMP-7 29.5 ± 0.5 g) did not differ, confirming that none of the treatment modalities affected the diabetic metabolism in mice per se. In all groups (treated and untreated), the mortality was ~30% between 2 and 4 months after the single STZ injection. Deaths before 2 months were not noted in any groups, ruling out any acute toxicity. Some previous studies have suggested that the STZ dose administered in our study might be toxic. In this regard, we believe that the outbred CD1 mice might be more resilient than the inbred strain of mice. We in fact found more toxicity when C57BL/6 mice were used. The outbred CD1 mice are larger than the inbred mice at the same age and thus might be able to withstand the effects of STZ much better than the inbred C57BL/6 mice.

DISCUSSION

Diabetic nephropathy is a leading cause of ESRD worldwide. Progress in evaluating the underlying pathogenic pathways and development of new therapeutic strategies has been impaired because of the lack of representative animal models mimicking human diabetic nephropathy. Here, we report that CD1 mice developed chronic renal disease associated with tubulointerstitial fibrosis and decreased renal excretory function within 6 months after a single injection of STZ. Interestingly, C57BL/6 and 129Sv mouse strains did not develop interstitial fibrosis, but they

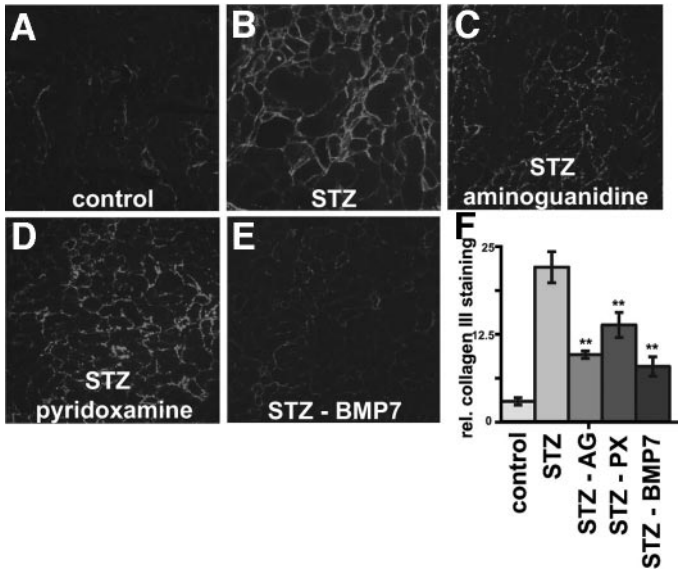

FIG. 6. Collagen III accumulation. Kidney tissues from nondiabetic CD1 mice (control), STZ-injected diabetic CD1 mice, and STZ-injected diabetic CD1 mice that received either aminoguanidine, pyridoxamine, or rhBMP-7 were stained with antibodies specific to collagen III. Relative stained area was quantified using National Institutes of Health ImageJ software. The pictures display representative photomicrographs of each group (*A–E*). The bar graph summarizes average values of each group (*F*). Administration of aminoguanidine, pyridoxamine, or rhBMP-7 led to significant decrease of collagen III accumulation as compared with untreated STZ-diabetic mice. **$P < 0.01$ vs. STZ group. AG, aminoguanidine; PX, pyridoxamine.

exhibited prominent glomerular lesions, increased blood glucose levels, and albuminuria, comparable to STZ-induced diabetic CD1 mice. Although our study does not address the mechanistic reason behind such differences, they reiterate the importance of genetic background in diabetic nephropathy progression. Among the advantages of this new mouse model are that it recapitulates several pathologies associated with human diabetic nephropathy.

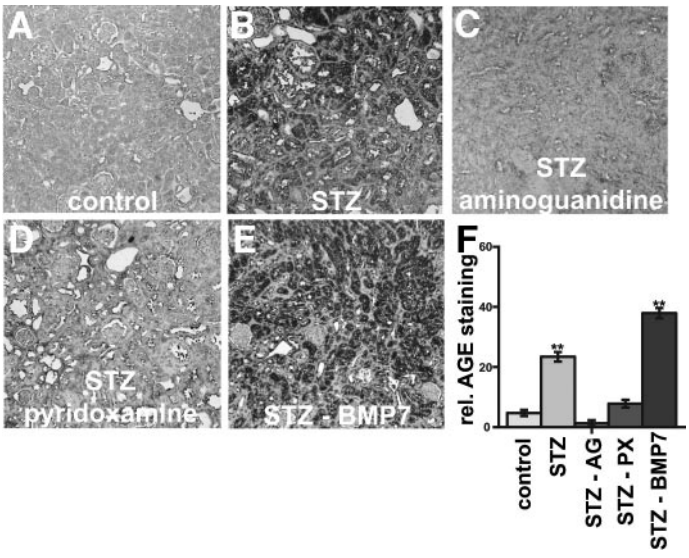

FIG. 7. AGE accumulation. Kidney tissues from nondiabetic CD1 mice (control), STZ-injected diabetic CD1 mice, and STZ-injected diabetic CD1 mice that received either aminoguanidine, pyridoxamine, or rhBMP-7 were stained with antibodies specific to CML. Positive staining was visualized using the CSAII biotin–free tyramide signal amplification system resulting in a brown precipitate. Although administration of the AGE inhibitors aminoguanidine and pyridoxamine both reduced accumulation of the CML-AGE, treatment with rhBMP-7 did not affect AGE accumulation compared with untreated STZ-induced diabetic mice. The pictures display representative pictures of each group at an original magnification of 10×, and the bar graph summarizes the digital quantification of staining for each group. **$P < 0.01$ vs. STZ group. AG, aminoguanidine; PX, pyridoxamine.

We further provide evidence that each of the experimental therapeutics—aminoguanidine, pyridoxamine, and rhBMP-7—are effective in inhibiting the progression of renal disease in STZ-induced diabetic CD1 mice. Aminoguanidine and pyridoxamine inhibit glomerular disease in STZ-induced diabetic CD1 mice, whereas rhBMP-7 inhibits predominantly tubulointerstitial fibrosis. Our results demonstrate that pyridoxamine does not offer any advantage over aminoguanidine in inhibiting diabetic nephropathy. In addition to inhibition of AGE formation, aminoguanidine is known as an effective free radical scavenger (31), and pyridoxamine has the capacity to scavenge toxic carbonyl products (32). Thus, whereas both aminoguanidine and pyridoxamine inhibit AGE accumulation, additional beneficial properties cannot be excluded. Our findings suggest that combination of an AGE inhibitor and BMP-7 can provide synergistic effects in the clinic and argue for combining them in human clinical trials.

ACKNOWLEDGMENTS

This study was supported in part by research grants DK62987 and DK55001 from the National Institutes of Health, a research fund from the Beth Israel Deaconess Medical Center for the Division of Matrix Biology, and a Stop and Shop Pediatric Tumor Foundation fellowship from Dana-Farber Cancer Institute (DFCI) (to H.S.). M.Z. was funded by a grant from the National Institutes of Health (5K08DK074558-01) and a American Society of Nephrology Carl W. Gottschalk Award.

REFERENCES

1. Ritz E, Rychlik I, Locatelli F, Halimi S: End-stage renal failure in type 2 diabetes: a medical catastrophe of worldwide dimensions. *Am J Kidney Dis* 34:795–808, 1999
2. Fioretto P, Kim Y, Mauer M: Diabetic nephropathy as a model of reversibility of established renal lesions. *Curr Opin Nephrol Hypertens* 7:489–494, 1998
3. Fioretto P, Sutherland DE, Najafian B, Mauer M: Remodeling of renal interstitial and tubular lesions in pancreas transplant recipients. *Kidney Int* 69:907–912, 2006
4. Breyer MD, Bottinger E, Brosius FC 3rd, Coffman TM, Harris RC, Heilig CW, Sharma K: Mouse models of diabetic nephropathy. *J Am Soc Nephrol* 16:27–45, 2005
5. Young BA, Maynard C, Boyko EJ: Racial differences in diabetic nephropathy, cardiovascular disease, and mortality in a national population of veterans. *Diabetes Care* 26:2392–2399, 2003
6. Mauer SM, Lane P, Zhu D, Fioretto P, Steffes MW: Renal structure and function in insulin-dependent diabetes mellitus in man. *J Hypertens Suppl* 10:S17–S20, 1992
7. Sugimoto H, Shikata K, Wada J, Horiuchi S, Makino H: Advanced glycation end products-cytokine-nitric oxide sequence pathway in the development of diabetic nephropathy: aminoguanidine ameliorates the overexpression of tumour necrosis factor-alpha and inducible nitric oxide synthase in diabetic rat glomeruli. *Diabetologia* 42:878–886, 1999
8. Metz TO, Alderson NL, Thorpe SR, Baynes JW: Pyridoxamine, an inhibitor of advanced glycation and lipoxidation reactions: a novel therapy for treatment of diabetic complications. *Arch Biochem Biophys* 419:41–49, 2003
9. Zeisberg M, Bottiglio C, Kumar N, Maeshima Y, Strutz F, Muller GA, Kalluri R: Bone morphogenic protein-7 inhibits progression of chronic renal fibrosis associated with two genetic mouse models. *Am J Physiol Renal Physiol* 285:F1060–F1067, 2003
10. Sugimoto H, Hamano Y, Charytan D, Cosgrove D, Kieran M, Sudhakar A, Kalluri R: Neutralization of circulating vascular endothelial growth factor (VEGF) by anti-VEGF antibodies and soluble VEGF receptor 1 (sFlt-1) induces proteinuria. *J Biol Chem* 278:12605–12608, 2003

11. Sugimoto H, Mundel TM, Sund M, Xie L, Cosgrove D, Kalluri R: Bone-marrow-derived stem cells repair basement membrane collagen defects and reverse genetic kidney disease. *Proc Natl Acad Sci U S A* 103:7321–7326, 2006
12. Zeisberg M, Hanai J, Sugimoto H, Mammoto T, Charytan D, Strutz F, Kalluri R: BMP-7 counteracts TGF-beta1-induced epithelial-to-mesenchymal transition and reverses chronic renal injury. *Nat Med* 9:964–968, 2003
13. Brocco E, Fioretto P, Mauer M, Saller A, Carraro A, Frigato F, Chiesura-Corona M, Bianchi L, Baggio B, Maioli M, Abaterusso C, Velussi M, Sambataro M, Virgili F, Ossi E, Nosadini R: Renal structure and function in non-insulin dependent diabetic patients with microalbuminuria. *Kidney Int Suppl* 63:S40–S44, 1997
14. Kushiro M, Shikata K, Sugimoto H, Ikeda K, Horiuchi S, Makino H: Accumulation of Nsigma-(carboxy-methyl)lysine and changes in glomerular extracellular matrix components in Otsuka Long-Evans Tokushima fatty rat: a model of spontaneous NIDDM. *Nephron* 79:458–468, 1998
15. Leiter EH: Multiple low-dose streptozotocin-induced hyperglycemia and insulitis in C57BL mice: influence of inbred background, sex, and thymus. *Proc Natl Acad Sci U S A* 79:630–634, 1982
16. Mauer SM, Steffes MW, Ellis EN, Sutherland DE, Brown DM, Goetz FC: Structural-functional relationships in diabetic nephropathy. *J Clin Invest* 74:1143–1155, 1984
17. Chavers BM, Bilous RW, Ellis EN, Steffes MW, Mauer SM: Glomerular lesions and urinary albumin excretion in type I diabetes without overt proteinuria. *N Engl J Med* 320:966–970, 1989
18. Dalla Vestra M, Saller A, Bortoloso E, Mauer M, Fioretto P: Structural involvement in type 1 and type 2 diabetic nephropathy. *Diabetes Metab* 26 (Suppl. 4):8–14, 2000
19. Sharma K, Jin Y, Guo J, Ziyadeh FN: Neutralization of TGF-beta by anti-TGF-beta antibody attenuates kidney hypertrophy and the enhanced extracellular matrix gene expression in STZ-induced diabetic mice. *Diabetes* 45:522–530, 1996
20. Yamamoto Y, Maeshima Y, Kitayama H, Kitamura S, Takazawa Y, Sugiyama H, Yamasaki Y, Makino H: Tumstatin peptide, an inhibitor of angiogenesis, prevents glomerular hypertrophy in the early stage of diabetic nephropathy. *Diabetes* 53:1831–1840, 2004
21. Kume E, Doi C, Itagaki S, Nagashima Y, Doi K: Glomerular lesions in unilateral nephrectomized and diabetic (UN-D) mice. *J Vet Med Sci* 54:1085–1090, 1992
22. McGowan TA, Zhu Y, Sharma K: Transforming growth factor-beta: a clinical target for the treatment of diabetic nephropathy. *Curr Diab Rep* 4:447–454, 2004
23. Ziyadeh FN, Hoffman BB, Han DC, Iglesias-De La Cruz MC, Hong SW, Isono M, Chen S, McGowan TA, Sharma K: Long-term prevention of renal insufficiency, excess matrix gene expression, and glomerular mesangial matrix expansion by treatment with monoclonal antitransforming growth factor-beta antibody in db/db diabetic mice. *Proc Natl Acad Sci U S A* 97:8015–8020, 2000
24. Stitt A, Gardiner TA, Alderson NL, Canning P, Frizzell N, Duffy N, Boyle C, Januszewski AS, Chachich M, Baynes JW, Thorpe SR: The AGE inhibitor pyridoxamine inhibits development of retinopathy in experimental diabetes. *Diabetes* 51:2826–2832, 2002
25. Metz TO, Alderson NL, Chachich ME, Thorpe SR, Baynes JW: Pyridoxamine traps intermediates in lipid peroxidation reactions in vivo: evidence on the role of lipids in chemical modification of protein and development of diabetic complications. *J Biol Chem* 278:42012–42019, 2003
26. Hruska KA, Guo G, Wozniak M, Martin D, Miller S, Liapis H, Loveday K, Klahr S, Sampath TK, Morrissey J: Osteogenic protein-1 prevents renal fibrogenesis associated with ureteral obstruction. *Am J Physiol Renal Physiol* 279:F130–F143, 2000
27. Lin J, Patel SR, Cheng X, Cho EA, Levitan I, Ullenbruch M, Phan SH, Park JM, Dressler GR: Kielin/chordin-like protein, a novel enhancer of BMP signaling, attenuates renal fibrotic disease. *Nat Med* 11:387–393, 2005
28. Wang S, Hirschberg R: Bone morphogenetic protein-7 signals opposing transforming growth factor beta in mesangial cells. *J Biol Chem* 279: 23200–23206, 2004
29. Zeisberg M: Bone morphogenic protein-7 and the kidney: current concepts and open questions. *Nephrol Dial Transplant* 21:568–573, 2006
30. Wang S, Chen Q, Simon TC, Strebeck F, Chaudhary L, Morrissey J, Liapis H, Klahr S, Hruska KA: Bone morphogenic protein-7 (BMP-7), a novel therapy for diabetic nephropathy. *Kidney Int* 63:2037–2049, 2003
31. Stoppa GR, Cesquini M, Roman EA, Ogo SH, Torsoni MA: Aminoguanidine prevented impairment of blood antioxidant system in insulin-dependent diabetic rats. *Life Sci* 78:1352–1361, 2006
32. Voziyan PA, Hudson BG: Pyridoxamine: the many virtues of a maillard reaction inhibitor. *Ann N Y Acad Sci* 1043:807–816, 2005